SOLUTION OF AEROACOUSTIC BENCHMARK PROBLEMS BY DISCONTINUOUS GALERKIN METHOD AND PERFECTLY MATCHED LAYER FOR NONUNIFORM MEAN FLOWS

Fang Q. Hu

Department of Mathematics and Statistics, Old Dominion University Norfolk, Virginia 23529 fhu@odu.edu

ABSTRACT

Numerical solutions of Problems 1 and 3 in Category 1 are presented. For Problem 1, the one-dimensional wave equation is solved by the discontinuous Galerkin method. Numerical dispersion and dissipation errors of the discontinuous Galerkin method are discussed and compared with finite difference schemes. For Problem 3, Perfectly Match Layer (PML) for the linearized Euler equations with a non-uniform mean flow is presented. The stable absorbing boundary condition is constructed based on a dispersive wave analysis of the normal modes of the Couette flow. Numerical results show excellent agreement with the exact solution. Solutions for both the subsonic and transonic Couette flow problems are presented.

ALIASING ERRORS

We solve the one-dimensional wave equation

$$\frac{\partial u}{\partial t} + \frac{\partial u}{\partial x} = 0 \tag{1}$$

with initial condition

$$u_0(x) = [2 + \cos(\alpha x)]e^{-(\ln 2)(x/10)^2}.$$
(2)

The value of α for the two cases specified in the problem is 1.7 and 4.6 respectively.

We first note that the Fourier transform of the initial condition (2) is

$$\hat{u}_0(k) = \frac{1}{2\pi} \int_{-\infty}^{\infty} u_0(x) e^{ikx} dx = \frac{10}{\sqrt{\pi \ln 2}} e^{-25k^2/\ln 2} + \frac{5}{2\sqrt{\pi \ln 2}} \left[e^{-25(k+\alpha)^2/\ln 2} + e^{-25(k-\alpha)^2/\ln 2} \right].$$

The Fourier transform is plotted in Figure 1. As we can see that, for the first case of $\alpha=1.7$, the numerical scheme is required to resolve accurately waves of as short a wavelength as three grid points (i.e., $k\Delta x\approx 2$, with gird spacing $\Delta x=1$). Although the resolution of a scheme generally improves as the order (or the number of stencil points) of the scheme increases, it may still require a scheme of an extraordinarily high order to satisfy the resolution requirement of this problem. This may not always be practical since the increase in the order of the scheme will increase the cost of computation as well.

On the other hand, Figure 1 clearly shows that there are two distinct parts in the initial condition, namely a smooth mean profile ($|k| \le 0.5$) and a highly oscillatory part ($1.5 \le |k| \le 2$). In this paper, we will not try to resolve the high oscillations under the specified grid, but rather the objective of our computation will be to preserve the mean profile accurately while at the same time eliminate the high-frequency oscillations. The numerical scheme to be used is the 4th-order discontinuous Galerkin (DG) scheme. We will illustrate that the discontinuous Galerkin method has a much better wave propagation properties than finite difference schemes of the same order and the built-in dissipation mechanism of the DG scheme can effectively damp out the high frequency oscillations[15, 12].

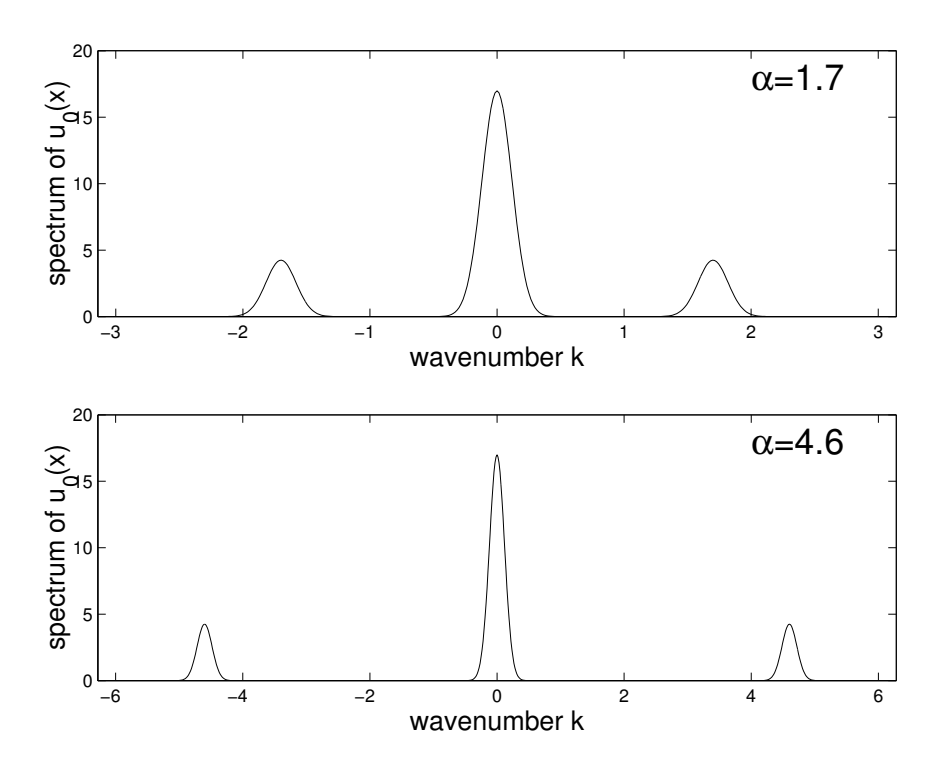


Figure 1: Fourier transform of the initial condition.

Discontinuous Galerkin method

Discontinuous Galerkin method is a finite element method that uses discontinuous basis functions[1, 3]. For the current problem, a computational domain of [-56, 960] is divided into 254 elements with a length of 4 for each element. Since the solution in each element will be represented by a polynomial of order 3(with four coefficients), the total number of degrees of freedom is equivalent to that of an explicit finite difference scheme using $\Delta x = 1$.

In each element $[x_n, x_{n+1}]$, where

$$x_n = -56 + 4n, \quad n = 0, 1, ..., 253,$$

the solution is approximated by an expansion in basis polynomials,

$$u_n(x,t) = \sum_{\ell=0}^{p} c_{\ell}^n(t)\phi_{\ell}(x).$$
 (3)

In (3), $\phi_{\ell}(x)$ is the basis function and $c_{\ell}^{n}(t)$ is the expansion coefficient. In this paper, Legendre polynomials are used for $\phi_{\ell}(x)$ and p=3.

A weak formulation of the wave equation (1) is

$$\int_{x_n}^{x_{n+1}} \frac{\partial u}{\partial t} v dx + \left[uv \right]_{x_n}^{x_{n+1}} - \int_{x_n}^{x_{n+1}} u \frac{\partial v}{\partial x} dx = 0$$
 (4)

where v is the test function[1, 3]. By substituting (3) into (4) and choosing the test function to be the basis functions, we get a system of semi-discrete equations as follows[1, 12],

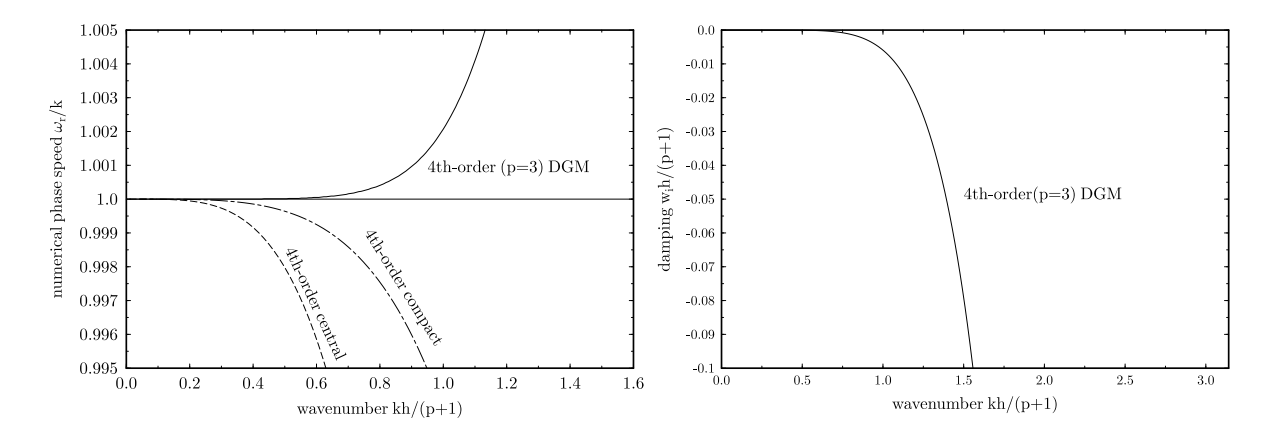


Figure 2: Left: numerical phase speed of the fourth-order DG and central difference schemes, compared using the wavenumber scaled by the degree of freedom; h is the element length and p is the order of basis polynomial in DG. Right: damping error of DG scheme.

$$\sum_{\ell=0}^{p} \frac{dc_{\ell}^{n}}{dt} \int_{x_{n}}^{x_{n+1}} \phi_{\ell}(x)\phi_{m}(x)dx + u^{n}(x_{n+1})\phi_{m}(x_{n+1}) - u^{n-1}(x_{n})\phi_{m}(x_{n}) - \sum_{\ell=0}^{p} c_{\ell}^{n} \int_{x_{n}}^{x_{n+1}} \phi_{\ell} \frac{d\phi_{m}}{dx} dx = 0$$
(5)

for m = 0, 1, ..., p.

This is a system of ordinary differential equations for the expansion coefficients $c_\ell^n(t)$. It is solved numerically by the optimized low-dissipation and low-dispersion Runge-Kutta scheme (LDDRK[14]). In particular, the optimized 5- and 6-stage combined scheme (LDDRK 5-6) is used. This scheme is formally fourth-order and has been optimized to have larger accuracy and stability limits than single-stage optimized schemes.

The discontinuous Galerkin method does not require a uniform mesh and works naturally with unstructured grids in two and three space dimensions. Unlike the continuous finite element method, there is no global matrix to be inverted which make the method highly efficient for parallel computing.

Recent Fourier analysis of the semi-discrete equation (5) shows that DG schemes are super-accurate for wave propagations[12, 13]. That is, for a scheme using polynomials of order p, the numerical dispersion relation of the semi-discrete equation is accurate to order 2p + 2. For example, for the 4th-order DG scheme (employing third order polynomials) used in the present problem, the numerical phase speed is actually accurate to the 8th-order. In Figure 2 (left), we plot the phase speed of the 4th-order DG scheme as well as that of 4th-order explicit central and compact finite difference schemes, where the horizontal axis has been scaled to keep the degrees of freedom the same for a fair comparison. Clearly, the DG scheme preserves the phase speed much better than the finite difference schemes of the same order.

Due to upwinding at element interfaces, the DG scheme also has a built-in dissipation for high frequency waves [15, 12]. Figure 2 (right) shows the numerical damping rate of the 4ht-order DG scheme. The damping rate is also 8th-order accurate, i.e., proportional to $(kh)^{2p+2}$.

Numerical results

The numerical solution is initialized by a projection of the initial condition (2) onto the basis functions. Specifically, the initial state for element $[x_n, x_{n+1}]$ is obtained by

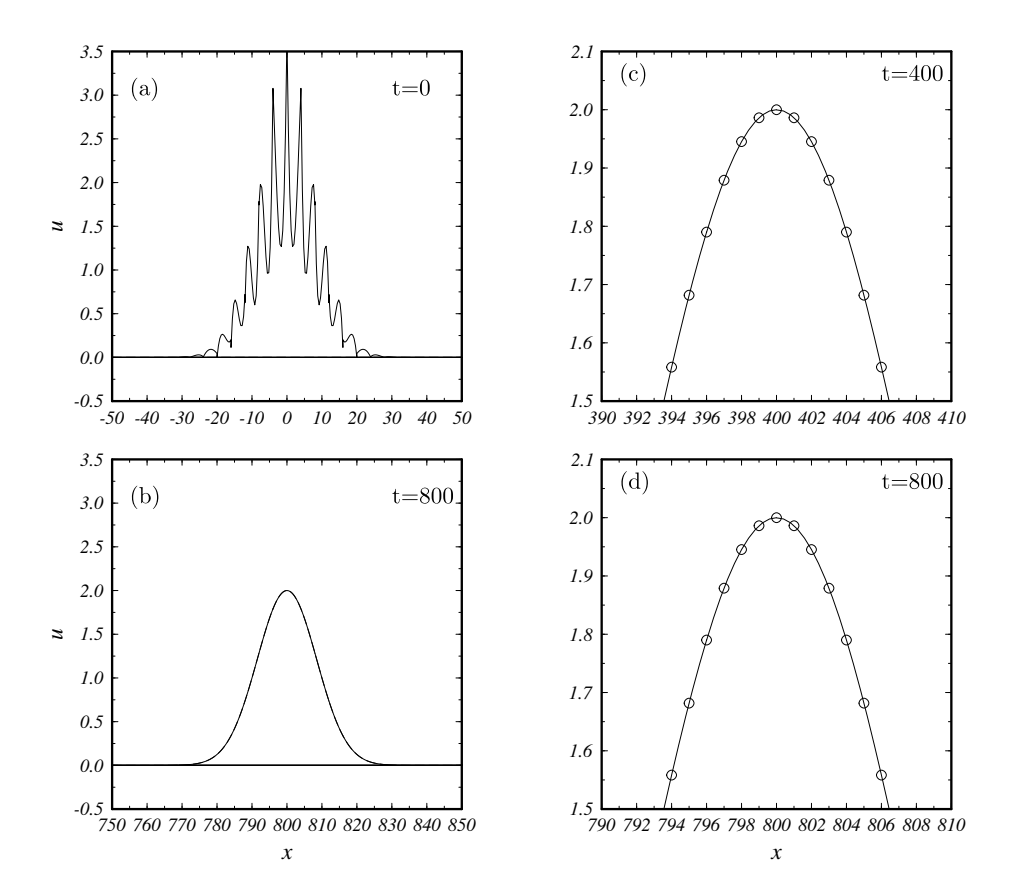


Figure 3: Numerical results of case I, $\alpha = 1.7$. (a) initial condition by projection process (7); (b) numerical solution at t = 800; (c) and (d) comparison with exact solution (without the oscillation part) at t = 400 and 800 respectively.

$$u_n(x,0) = \sum_{\ell=0}^{p} c_{\ell}^n(0)\phi_{\ell}(x)$$
 (6)

where $c_{\ell}^{n}(0)$ is computed by the requirement that

$$\int_{x_n}^{x_{n+1}} u_0(x)\phi_m(x)dx = \sum_{\ell=0}^p c_\ell^n(0) \int_{x_n}^{x_{n+1}} \phi_\ell(x)\phi_m(x)dx \tag{7}$$

for m = 0, 1, ..., p. The integral on the left hand side of (7) is carried out by a 20-point Gaussian quadrature rule and the integral on the right hand side is evaluated exactly.

Case I,
$$\alpha = 1.7$$

Figure 3(a) shows the projected initial condition. Since the DG scheme does not enforce continuity at element interfaces, discontinuities at element boundaries are expected when the function is not well resolved, which is the case for the highly oscillatory part of the initial condition. Figure 3(b) shows the solution at time t=800. The high frequency oscillations are effectively damped out and a smooth mean solution is seen. In Figures 3(c) and 3(d), we plot the numerical solution with the exact solution (without the oscillation part, in circles), at t=400 and 800 respectively. Clearly, the DG scheme preserves the mean Gaussian profile very well and the built-in dissipation affects only the unresolved high wavenumbers.

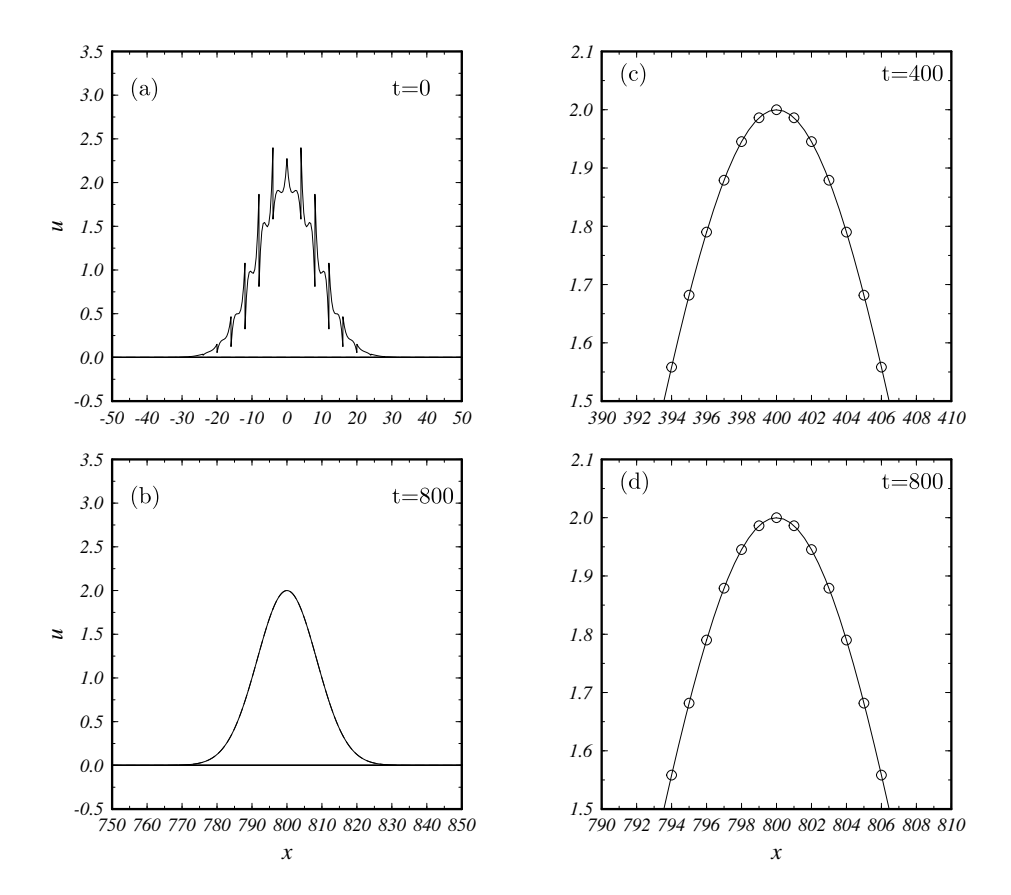


Figure 4: Numerical results of case II, $\alpha = 4.6$. (a) initial condition by projection process (7); (b) numerical solution at t = 800; (c) and (d) comparison with exact solution (without the oscillation part) at t = 400 and 800 respectively.

Case II, $\alpha = 4.6$

For the second case of $\alpha=4.6$, the projected initial condition is shown in Figure 4(a). We note that, unlike grid-based finite difference methods, the initial condition is not "aliased" with a lower wavenumber, because the projection process (7) "sees" the initial condition as a "continuous" function.

Figure 4(b) shows the solution at t = 800 and Figures 4(c) and 4(d) show the numerical and exact (without the oscillation part) solutions. Again, the high oscillations in the initial condition are damped out and, at the same time, the mean profile if accurately preserved.

PERFECTLY MATCHED LAYER FOR A NONUNIFORM MEAN FLOW

In Problem 3, nonreflecting boundary conditions are needed at the inflow and outflow boundaries of the channel Couette flow. In our computation, Perfectly Matched Layer (PML) will be used as absorbing boundary conditions so that out-going waves are attenuated with minimal reflection (Figure 5). We will discuss the construction of a stable PML equation for a non-uniform mean flow and present the numerical results.

The linearized Euler equation with a non-uniform mean flow is

$$\frac{\partial \mathbf{u}}{\partial t} + \mathbf{A} \frac{\partial \mathbf{u}}{\partial x} + \mathbf{B} \frac{\partial \mathbf{u}}{\partial y} + \mathbf{C} \mathbf{u} = 0$$
 (8)

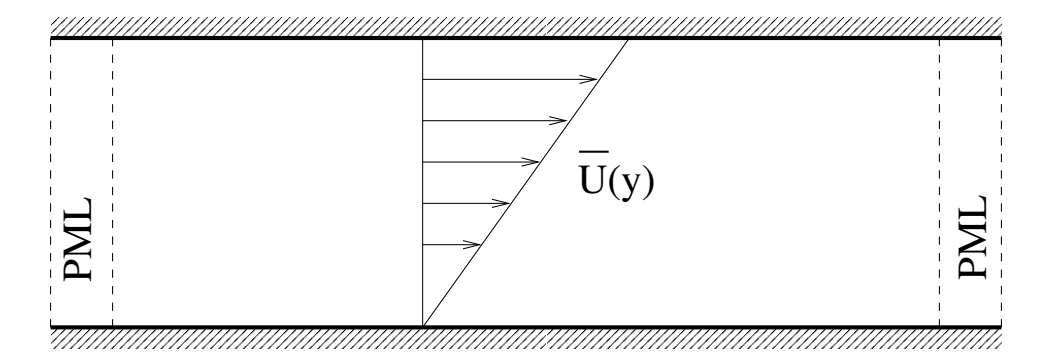


Figure 5: Schematic of Couette flow with PML absorbing boundary condition

where

$$\mathbf{u} = \begin{pmatrix} \rho \\ u \\ v \\ p \end{pmatrix}, \ \mathbf{A} = \begin{pmatrix} \bar{U} & 1 & 0 & 0 \\ 0 & \bar{U} & 0 & 1 \\ 0 & 0 & \bar{U} & 0 \\ 0 & 1 & 0 & \bar{U} \end{pmatrix}, \ \mathbf{B} = \begin{pmatrix} 0 & 0 & 1 & 0 \\ 0 & 0 & 0 & 0 \\ 0 & 0 & 0 & 1 \\ 0 & 0 & 1 & 0 \end{pmatrix}, \ \mathbf{C} = \begin{pmatrix} 0 & 0 & 0 & 0 \\ 0 & 0 & \frac{d\bar{U}}{dy} & 0 \\ 0 & 0 & 0 & 0 \\ 0 & 0 & 0 & 0 \end{pmatrix}$$

For the subsonic case, the mean flow is given by $\bar{U}(y) = 0.9y$ in a physical domain of $(x,y) \in [-2,2] \times [0,1]$. The mean density has been assumed to be constant. Solid wall boundary conditions are applied at y=0,1.

The Perfectly Matched Layer (PML) technique can be viewed as a complex change of variables when the governing equation is written in the frequency domain[6, 4, 21, 9]. For the present case, since only vertical absorbing layers are needed for non-reflecting boundary conditions, the derivation of the PML equation for (8) would involve a complex change of variable for x as follows,

$$x \to x + \frac{i}{\omega} \int_{x_0}^x \sigma_x dx \tag{9}$$

where σ_x is an arbitrary positive function of x and x_0 is the location of the interface between the Euler and PML domains.

However, in order to avoid generating instability waves in the PML equation, it has been found necessary to apply a *proper* space-time coordinate transformation to the Euler equation before applying the PML complex change of variable (9)[9]. Such a space-time transformation is important because any wave of the Euler equation having opposite signs in its phase and group velocities will result in instability of the PML equation[18, 9, 2]. That is, the phase and group velocities have to be consistent and have the same sign in order to maintain the stability of the PML equation. In a recent paper[2], this necessary condition for stable PML equation was stated mathematically as

$$\frac{\omega}{k} \frac{d\omega}{dk} \ge 0 \tag{10}$$

where k is the wavenumber in the x direction. The purpose of the space-time transformation is to ensure that in the transformed space-time coordinates, all waves have consistent phase and group velocities and satisfy condition (10). For the Euler equation with a *uniform* mean flow, the proper space-time transformation was found to be

$$\bar{x} = x, \quad \bar{t} = t + \beta x, \text{ with } \beta = \frac{\bar{U}_0}{1 - \bar{U}_0^2}$$
 (11)

where \bar{U}_0 is the mean flow Mach number[9]. The corresponding transformation in the frequency-wavenumber space is

$$\bar{k} = k + \beta \omega, \quad \bar{\omega} = \omega.$$
 (12)

It was shown in [9] that, in the transformed coordinates, all linear waves associated with the Euler equation of a uniform mean flow \bar{U}_0 have their phase and group velocities in the same direction. The importance of the transformation (11) and the particular choice for β have been confirmed independently in recent works in [2, 7, 8].

Now to construct the PML equation for Euler equation (8) with a *nonuniform* mean flow, let's first examine the *physical* waves associated with (8) and their dispersion relations. For this purpose, a dispersive wave analysis of (8) will be carried out. Specifically, we let

$$\mathbf{u} = \hat{\mathbf{u}}(y)e^{i(kx-\omega t)}$$

in Euler equation (8) and get

$$-i\omega\hat{\mathbf{u}} + ik\mathbf{A}\hat{\mathbf{u}} + \mathbf{B}\frac{d\hat{\mathbf{u}}}{dy} + \mathbf{C}\hat{\mathbf{u}} = 0.$$
(13)

Together with the homogeneous boundary conditions at $y = \pm 1$, (13) forms an eigenvalue problem for ω for any given value of k. The eigensolutions are called normal modes in the theory of hydrodynamic stability analysis[5]. This eigenvalue problem has been solved numerically by a spectral collocation method using Chebyshev polynomials[16]. It yields a complete spectrum of the waves supported by (13).

Figure 6 shows the dispersion relation diagram of all the normal modes of (13), i.e., real part of ω v.s. k. The imaginary part of ω is found to be zero for all modes, indicating that the Couette flow does not have physical instability wave. In the dispersion diagram, we see two families of waves. One family has phase speed between $U_{min}=0$ and $U_{max}=0.9$, shown between dashed lines in the ω_r-k diagram. These are "vortical" modes that convect with the mean flow. They are non-dispersive waves, i.e., $\omega/k=constant$ [22]. For these waves, condition (10) is satisfied. The other family of modes are "acoustic" modes[19, 17]. A closer examination of the acoustic modes indicates that they have a phase speed supersonic relative to part of the mean flow. They are dispersive waves.

Figure 6 indicates that the acoustic modes do not always have consistent phase and group velocities. A triangle on the acoustic modes denotes the location where the group velocity is zero. As we can see, for the acoustic modes in the upper left and lower right quarters in Figure 6 that lie between the triangle and the vertical axis, their phase velocity (ω_r/k) is negative but their group velocity $(d\omega_r/dk)$ is positive. As we have explained earlier, applying the PML complex change of variable (9) to the Euler equation (8) without the a proper space-time coordinate transformation will result in these waves being amplified and becoming unstable modes.

Therefore, we would seek a proper space-time transformation so that condition (10) is satisfied in the transformed coordinates.

Remarkably, the locations of points of zero group velocity on the dispersion diagram (Triangles in Figure 6) appear to lie nearly on a straight line! Inspection of points of zero group velocity shows a line of $\omega_r = ck_x$ where the slope of the line is approximately c = -1.85. Considering (12), this suggests a space-time coordinate transformation of the form (11) with the value for β determined by

$$\beta = -\frac{1}{c}.\tag{14}$$

This gives $\beta = 0.54$ or equivalently a value of $\bar{U}_0 = 0.437$ in (11).

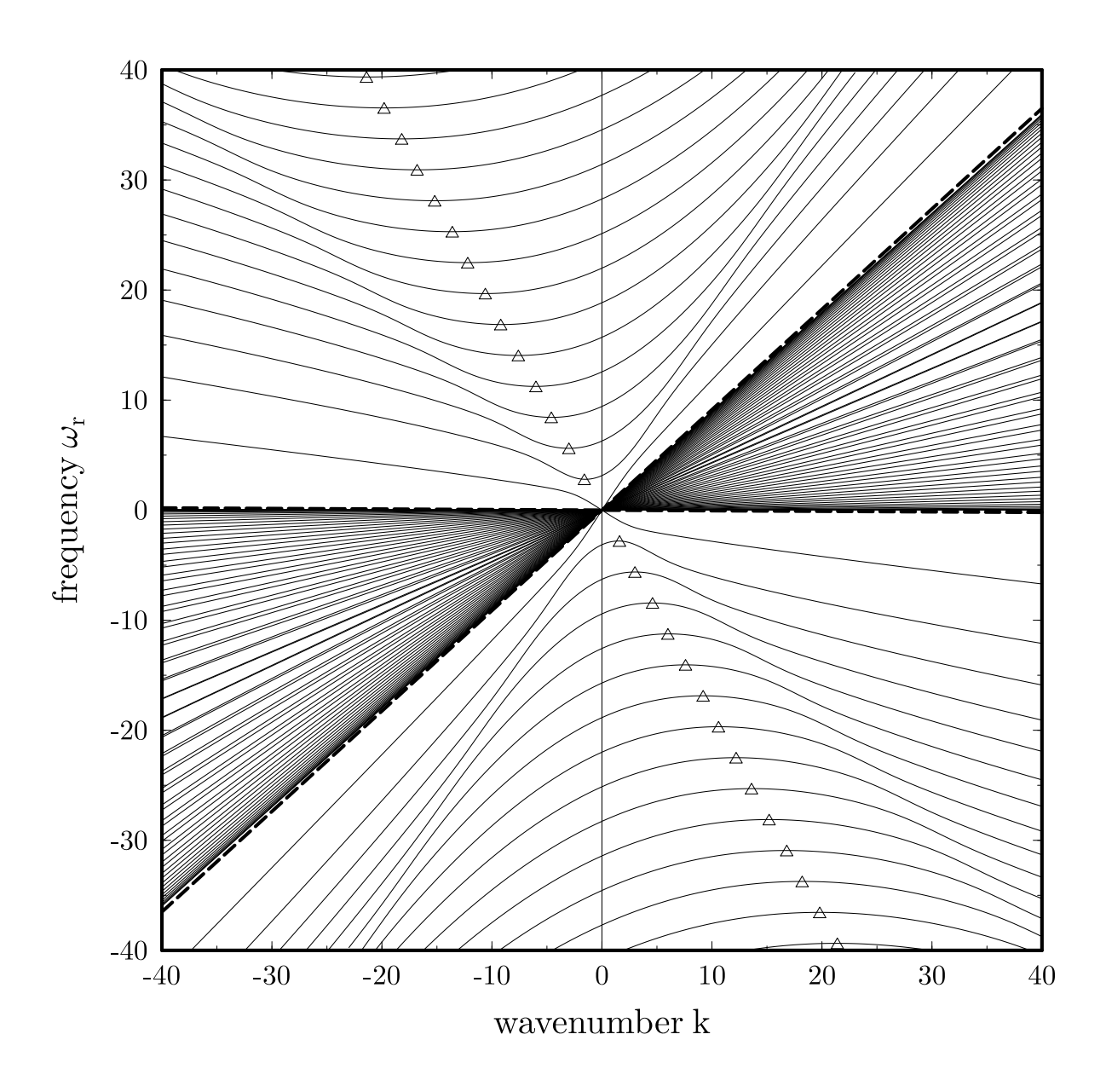


Figure 6: Dispersion relation diagram of physical wave. Triangles denote the points of zero group velocity.

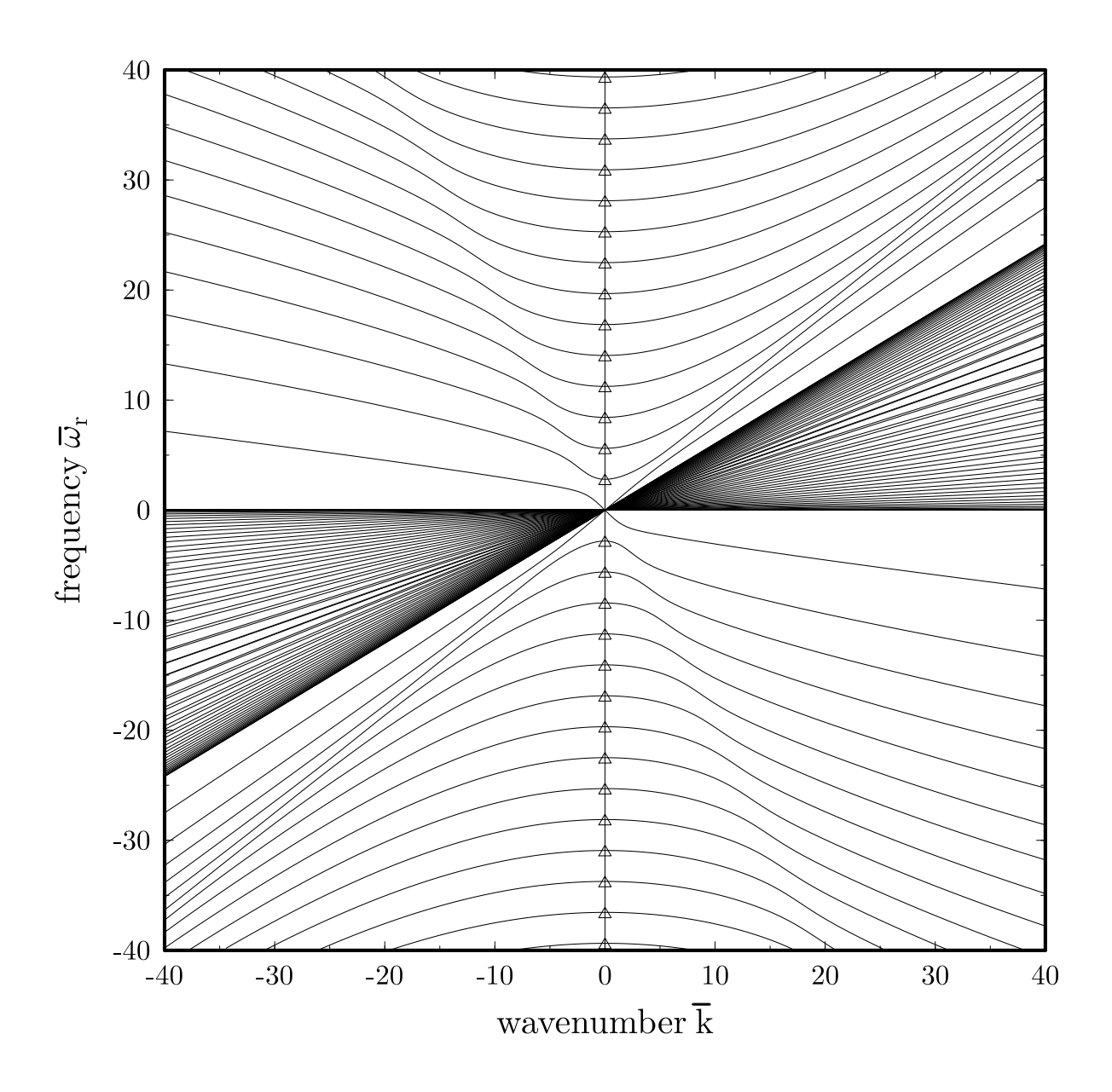


Figure 7: Dispersion relation diagram after applying the space-time transformation.

In Figure 7, we show the dispersion relation diagram in frequency-wavenumber space of the transformed coordinates. Indeed, we see that the phase and group velocities of all waves are consistent and the necessary condition (10) is now satisfied by all wave modes.

Once the value for β is chosen, the derivation of PML equation is similar to that of a uniform mean flow given in [9]. After the space-time transformation (11), the Euler equation in the frequency domain becomes

$$-i\bar{\omega}(\mathbf{I}+\beta\mathbf{A})\tilde{\mathbf{u}} + \mathbf{A}\frac{\partial \tilde{\mathbf{u}}}{\partial \bar{x}} + \mathbf{B}\frac{\partial \tilde{\mathbf{u}}}{\partial \bar{y}} + \mathbf{C}\tilde{\mathbf{u}} = 0.$$

By a complex change of variable of the form (9) for \bar{x} , we get the following PML equation in the frequency domain,

$$-i\bar{\omega}(\mathbf{I}+\beta\mathbf{A})\tilde{\mathbf{u}} + \mathbf{A}\frac{1}{1+\frac{i\sigma_x}{\bar{\omega}}}\frac{\partial\tilde{\mathbf{u}}}{\partial\bar{x}} + \mathbf{B}\frac{\partial\tilde{\mathbf{u}}}{\partial\bar{y}} + \mathbf{C}\tilde{\mathbf{u}} = 0.$$

Multiplying $1 + \frac{i\sigma_x}{\bar{\omega}}$, we get

$$(-i\bar{\omega} + \sigma_x)(\mathbf{I} + \beta \mathbf{A})\tilde{\mathbf{u}} + \mathbf{A}\frac{\partial \tilde{\mathbf{u}}}{\partial \bar{x}} + (1 + \frac{i\sigma_x}{\omega})\mathbf{B}\frac{\partial \tilde{\mathbf{u}}}{\partial \bar{y}} + (1 + \frac{i\sigma_x}{\omega})\mathbf{C}\tilde{\mathbf{u}} = 0.$$

This can be readily re-written in the original physical time domain as follows

$$\frac{\partial \mathbf{u}}{\partial t} + \mathbf{A} \frac{\partial \mathbf{u}}{\partial x} + \mathbf{B} \frac{\partial \mathbf{u}}{\partial y} + \sigma_x \mathbf{B} \frac{\partial \mathbf{q}}{\partial y} + \mathbf{C}(\mathbf{u} + \sigma_x \mathbf{q}) + \sigma_x \mathbf{u} + \sigma_x \beta \mathbf{A} \mathbf{u} = 0$$
 (15)

where

$$\frac{\partial \mathbf{q}}{\partial t} = \mathbf{u}.\tag{16}$$

Here, \mathbf{q} is an auxiliary variable vector. It is only needed inside the PML domain[9]. We note that this version of PML is almost identical to that given in [9] for the uniform mean flow, except for the term involving the C matrix. The value for β given by (14) is crucial for the stability of (15)-(16).

It is important to note that the fact that points of zero group velocity on the dispersion relation diagram fall on a line is not accidental. The same has been found in other types of subsonic mean flow velocity profiles, including mixing layers, jets and wakes[11]. In most cases, the value for β is found to be close to that given by (11) when \bar{U}_0 is taken to be the average of $\bar{U}(y)$. Therefore, PML equations (15)-(16) can be applied to a broad class of nonuniform mean flows. More examples will be presented in [11].

Numerical results

A computational domain of $[-2.15625, 2.15625] \times [0, 1]$ is discretized by a uniform grid of 553×129 points with $\Delta x = \Delta y = 1/128$ and 20 grid points in PML domains at the inflow and outflow. The spatial derivatives are approximated by the 7-point DRP scheme[20] and the time integration is carried out by the optimized 5- and 6-stage combined low-dissipation and low-dispersion Runge-Kutta scheme (LDDRK5-6[14]). A 10-th order filter has also been applied to limit the oscillations from the thin density wave in the problem.

The absorption coefficient in the PML domain varies with x as follows,

$$\sigma_x = \frac{4}{\Delta x} \left| \frac{x - x_0}{D} \right|^2$$

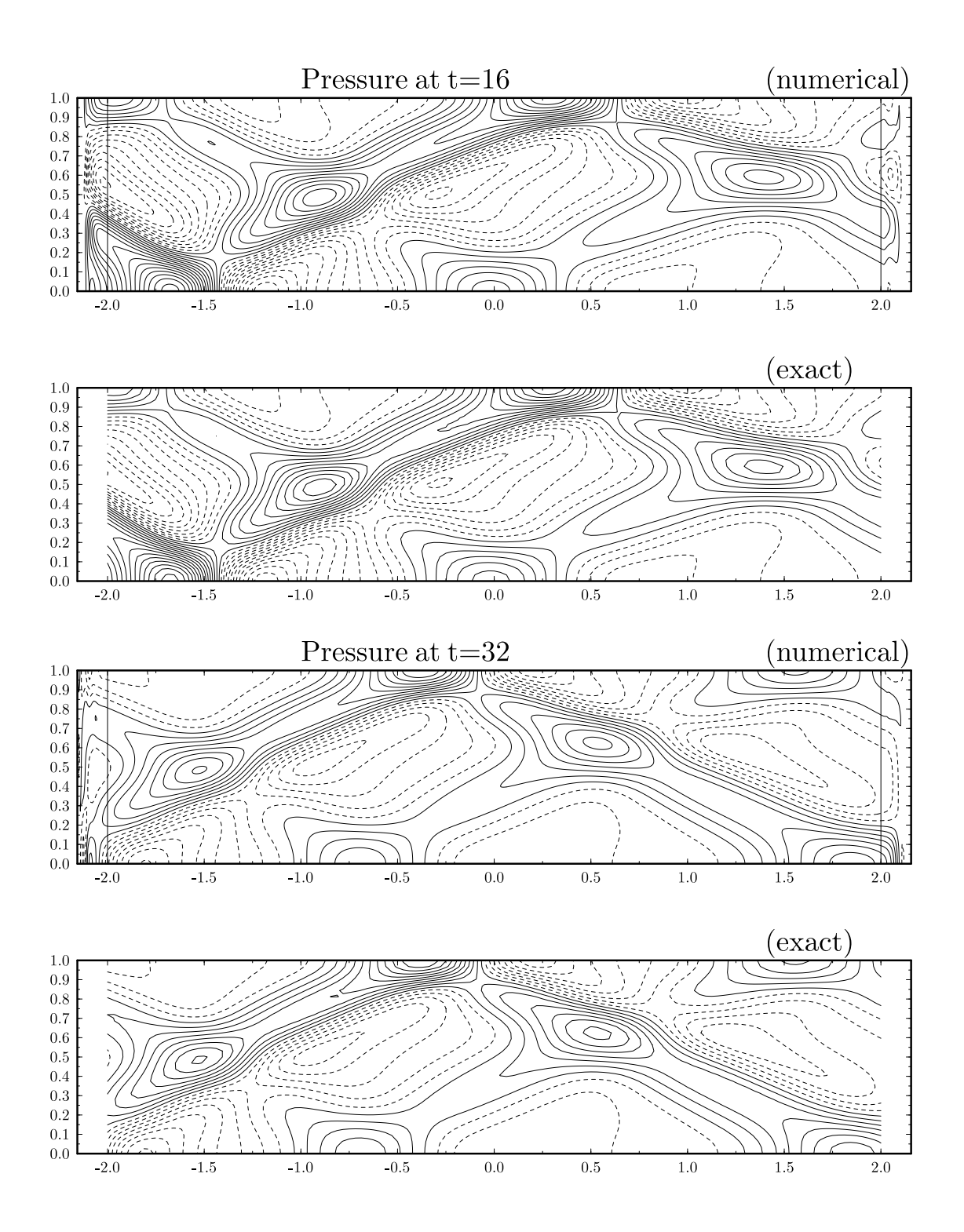


Figure 8: Pressure contours at t = 16 and 32.

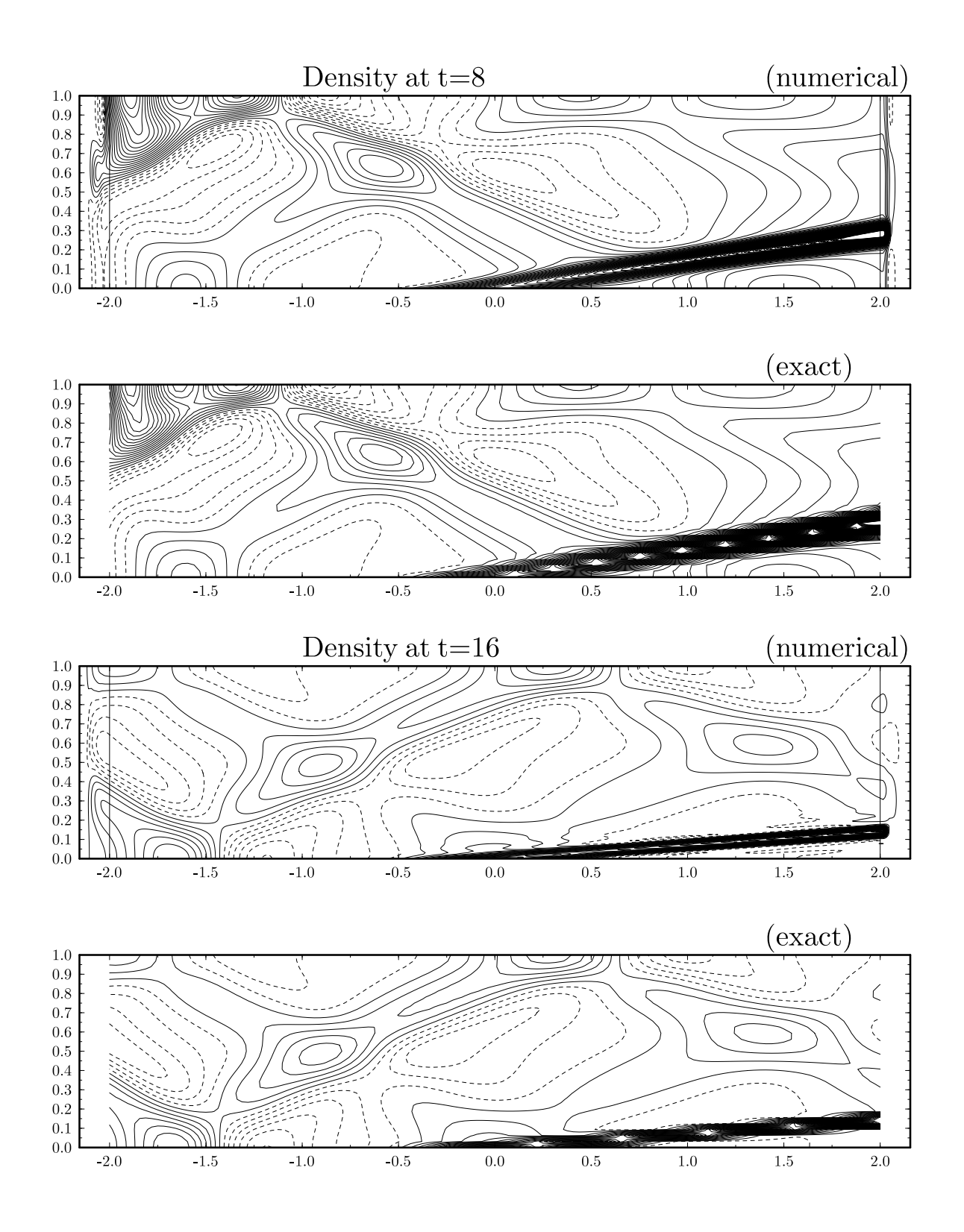


Figure 9: Density contours at t = 8 and 16.

where x_0 denotes the interface of the Euler and PML domains and D is the width of the PML domain, i.e., $D = 20\Delta x$ for the cases reported here.

A grid stretching inside the PML will also improve the effectiveness of the PML because the total absorption rate depends directly on the width of the PML domain[10]. On the other hand, we do not need the solutions inside the PML to be very accurate. The grid stretching is equivalent to modifying the x derivative term of the PML equation as

$$\frac{\partial}{\partial x} \to \frac{1}{\alpha(x)} \frac{\partial}{\partial x}$$

where $\alpha(x) \geq 1$ is a smooth function[10]. We have used the following expression for $\alpha(x)$ in our calculations,

$$\alpha(x) = 1 + 2 \left| \frac{x - x_0}{D} \right|^2.$$

Figure 8 shows the pressure contours of the numerical and exact solutions at t=16 and 32. The numerical solution decays exponentially inside the PML domain with very little reflection. Even with only 20 grid points in the PML domain, the agreements on contours between the numerical and exact solutions are excellent. Figure 9 shows the density contours at t=8 and 16. The absorption of the density pulse by the PML domain is clearly shown. We note that the initial density pulse is stretched thin by the shear mean flow and becomes less well resolved by the 7-point finite difference scheme at t=16 and beyond. Although there are some oscillations near the density wave, the overall contours compare well with the exact solution.

In Figure 10, the relative errors between the numerical and exact solutions are plotted as a function of time. The errors are computed as specified in the workshop problem, namely,

$$E_p = \frac{\|p - p_{exact}\|_2}{\|p_{exact}\|_2}, \qquad E_\rho = \frac{\|\rho - \rho_{exact}\|_2}{\|\rho_{exact}\|_2}$$
 (17)

for pressure E_p and density E_ρ . The error in pressure is less than 5% even with only 20 grid points in the PML domain. Since the L2 norm is carried out throughout the entire computational domain, The errors given by (17) actually include the numerical errors due to the boundary condition as well as the numerical discretization of the Euler equation. The larger error in the density is not due to the boundary condition, but reflects the fact that the thin density wave is not well resolved by the 7-point finite difference scheme used.

To further assess the error due to the boundary condition alone, we show in Figure 11 the error in density obtained by comparing the numerical solution with a *reference* solution which is computed using the same numerical scheme but a larger computational domain so it is not affected by the boundary condition. The relative error in density is now less than 1% up to t=64. It is further reduced to 0.2% when 30 grid points are used in the PML domain. To reduce computing time, the grid spacing is larger in this calculation, with $\Delta x = \Delta y = 1/32$.

TRANSONIC COUETTE FLOW

For the case of transonic Couette flow of U(y) = 1.2y, it becomes infeasible to use a space-time transformation of the form (11). The dispersion relations of all physical waves for this problem are plotted in Figure 12. There are now two points of zero group velocity for each acoustic mode. This is due to the fact that part of the mean flow is now supersonic. Therefore, a coordinate transformation of the form (11) will not be effective.

Since the mean flow is supersonic only in a narrow region of $5/6 \le y \le 1$, we have experimented with a "transition" zone over which the mean flow is modified gradually from supersonic to subsonic, and then

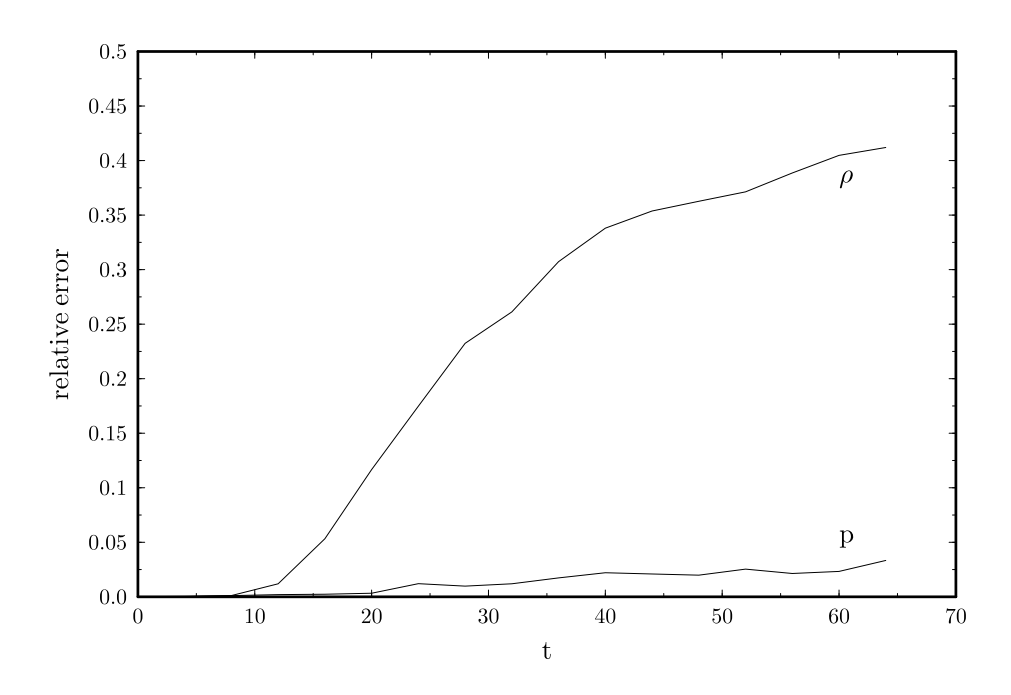


Figure 10: L2 norm of errors in pressure and density compared with the exact solution as defined in (17).

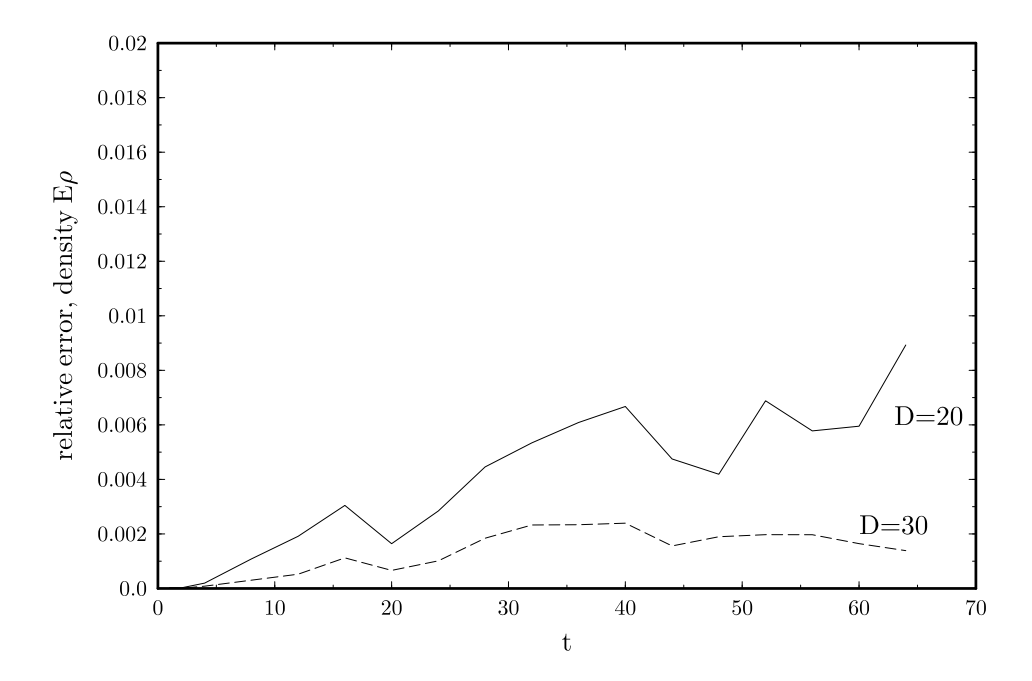


Figure 11: L2 norm of errors in density compared with reference solution. D indicates the number of grid points in side the PML domain.

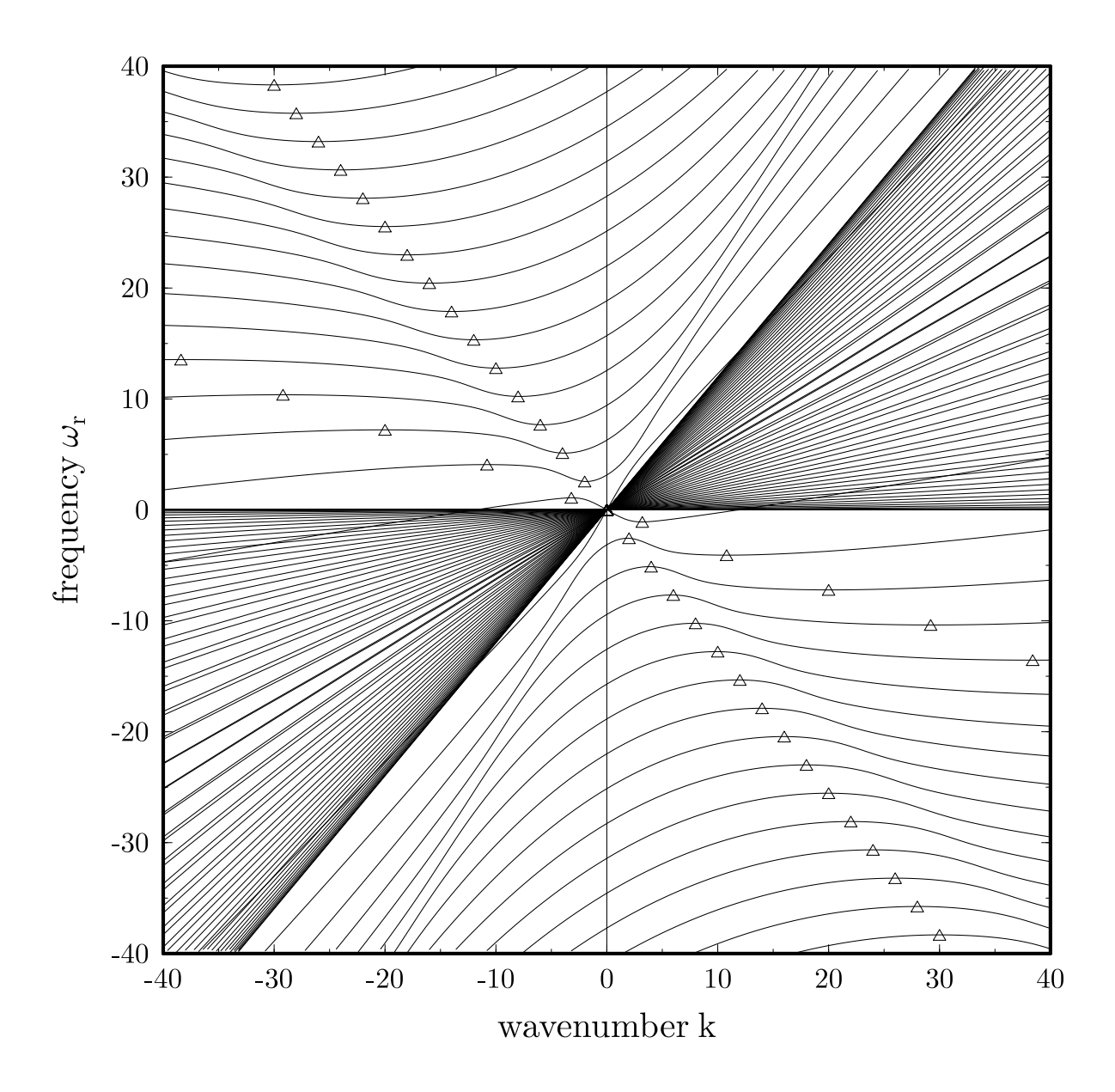


Figure 12: Dispersion diagram of the transonic flow. Triangles denote the points of zero group velocity.

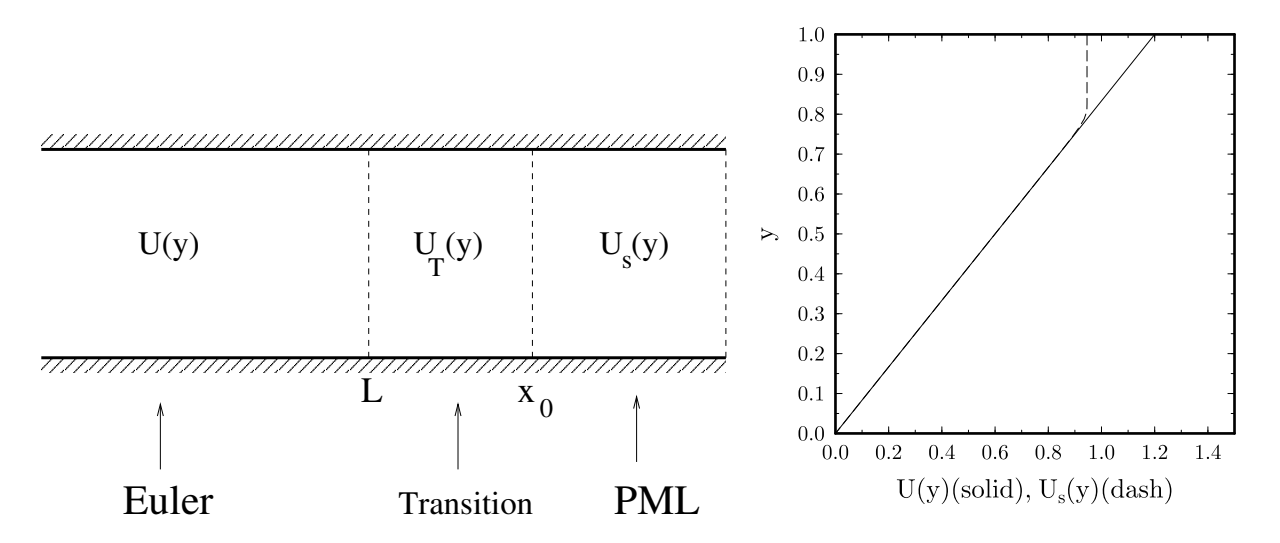


Figure 13: Left: a schematic showing a transition region from supersonic mean flow U(y) to a subsonic mean flow $U_s(y)$; Right: mean velocity for U(y), solid, and $U_s(y)$, dashed.

PML is applied to the subsonic mean flow, as shown in Figure 13. The result is not as good as in the previous case of subsonic flow, but it could be a practical solution as we will demonstrate below.

The subsonic mean velocity is given by

$$U_s(y) = \begin{cases} 1.2y(1 - e^{-(0.9 - y)/0.025}) & y < 0.8122\\ 0.9456 & y \ge 0.8122 \end{cases}$$

In the transition zone, the mean flow is morphed gradually from U(y) at x = L to $U_s(y)$ at $x = x_0$,

$$U_T(y) = (1 - \xi^2)U(y) + \xi^2 U_s(y)$$
, where $\xi = \frac{x - L}{x_0 - L}$.

Figure 14 shows the pressure contours at t=16 and t=32, together with the exact solutions. In this computation, we have used a uniform grid of $\Delta x=\Delta y=1/64$. The mean velocity transition zone has 20 grid points, with L=2.0 and $x_0=2.3125$. The PML domain has 20 grid points as well. Due to a relatively short span of the PML zone, there are visible reflected waves from the end of the PML zone. However, inside the physical domain, the agreements on the contours between the numerical and exact solutions are generally good. Of course the solution can be further improved by using more grid points in the transition and PML zones.

CONCLUSIONS

Numerical solutions to problems 1 and 3 in Category 1 have been presented. The calculation and analysis for Problem 1 show that the built-in dissipation mechanism of the discontinuous Galerkin method affects only the unresolved high frequency oscillations and leaves the resolved waves intact. For the Perfectly Matched Layer nonreflecting boundary condition, we have shown that it is possible to derive stable PML equation for the linearized Euler equation with a nonuniform mean flow based on a dispersive wave analysis of the physical wave system. The parameter in the PML equation is intimately linked to the dispersion relations of linear waves of the Euler equation. The PML shown in this paper is applicable to a broad class of nonuniform mean flows. Its extension to fully nonlinear Euler equation will be presented in a future work.

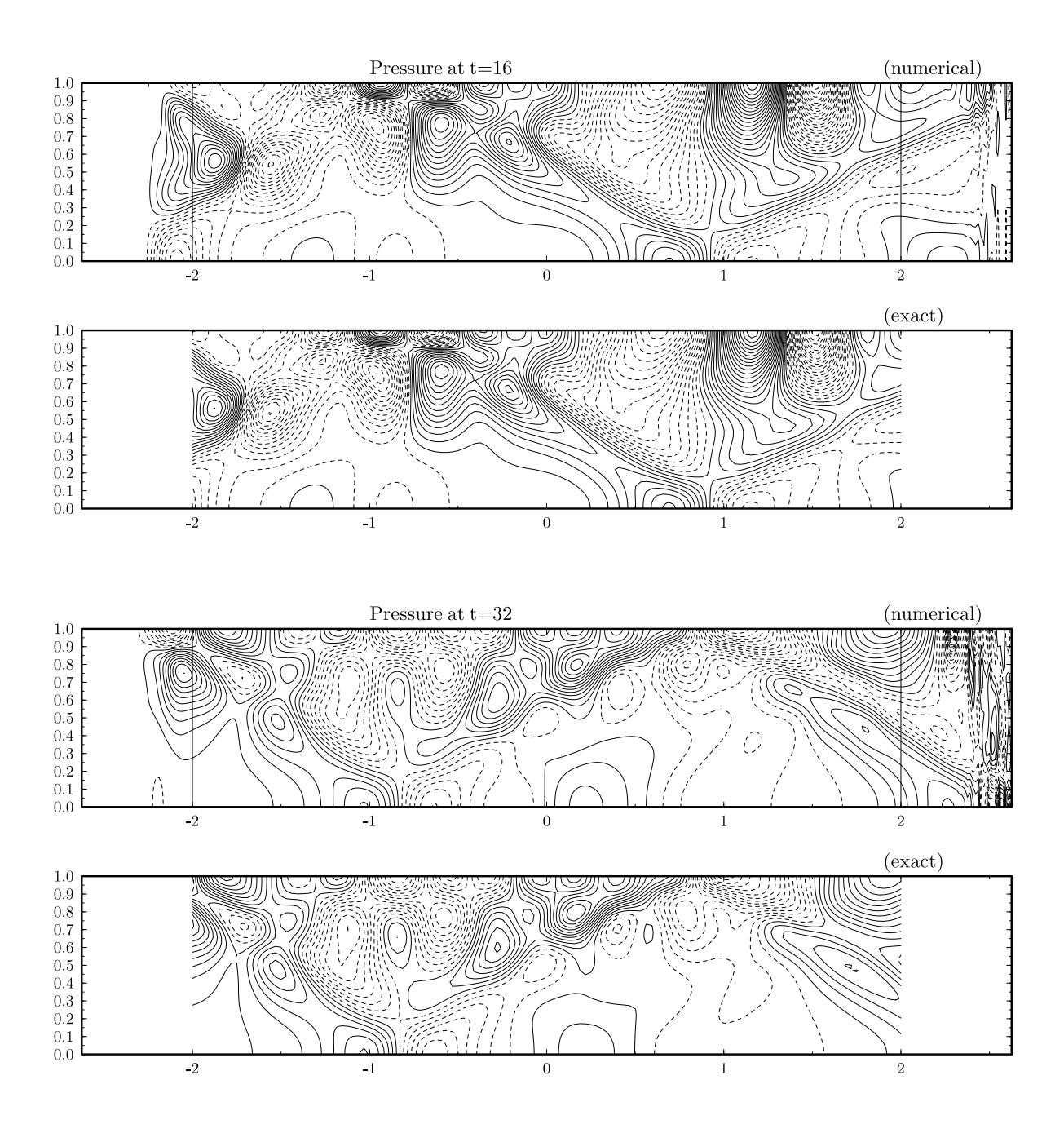


Figure 14: Pressure contours at t=16 and 32 for the transonic mean flow.

References

- [1] H. Atkins and C.-W. Shu, Quadrature-free implementation of discontinuous Galerkin methods for hyperbolic equations, *AIAA Journal*, Vol.36, 775-782, 1998.
- [2] E. Becache, S. Fauqueux and P. Joly, Stability of perfectly matched layers, group velocities and anisotropic waves, *Journal of Computational Physics*, Vol. 188, 399-433, 2003.
- [3] B. Cockburn and C.-W. Shu, The Runge-Kutta discontinuous Galerkin method for the conservation Laws V, *Journal of Computational Physics*, Vol. 141, 199-224, 1998.
- [4] F. Collino and P. Monk, The perfectly matched layer in curvilinear coordinates, *SIAM J. Sci, Comp*, Vol. 19, No. 6, P. 2016, 1998.
- [5] P. G. Drazin and W. H. Reid, *Hydrodynamic stability*, Cambridge University Press, 1981.
- [6] S. D. Gedney, An anisotropic perfectly matched layer-absorbing medium for the truncation of FDTD lattices, *IEEE Trans. Antennas Propagation*, Vol. 44, P. 1630, 1996.
- [7] T. Hagstrom and I. Nazarov, Absorbing layers and radiation boundary conditions for jet flow simulations, AIAA paper 2002-2606, 2002.
- [8] T. Hagstrom and I. Nazarov, Perfectly matched layers and radiation boundary conditions for shear flow calculations, AIAA paper 2003-3298, 2003.
- [9] F. Q. Hu, A stable, Perfectly Matched Layer for linearized Euler equations in unsplit physical variables, Journal of Computational Physics, Vol. 173, 455-480, 2001.
- [10] F. Q. Hu, Absorbing boundary conditions (a review), to appear in *International Journal of Computational Fluid Dynamics*, 2004.
- [11] F. Q. Hu, On using Perfectly Matched Layer for the Euler equations with a non-uniform mean flow, AIAA paper for the 10-th AIAA/CEAS Aeroacoustics Conference, 2004.
- [12] F. Q. Hu and H. L. Atkins, Eigensolution analysis of discontinuous Galerkin method. Part I, One space dimension, *Journal of Computational Physics*, Vol. 182, 516-545, 2002.
- [13] F. Q. Hu and H. L. Atkins, Two-dimensional wave analysis of the discontinuous Galerkin method with non-uniform grids and boundary conditions, AIAA-paper 2002-2514, 2002.
- [14] F. Q. Hu, M. Y. Hussaini and J. L. Manthey, Low dissipation and low dispersion Runge-Kutta schemes for computational acoustics, *Journal of Computational Physics*, Vol. 124, 177-191, 1996.
- [15] F. Q. Hu, M. Y. Hussaini and P. Rasetarinera, An analysis of the discontinuous Galerkin method for wave propagation problems, *Journal of Computational Physisc*, Vol. 151, 921-946, 1999.
- [16] F. Q. Hu and C. K. W. Tam, Parametric instability of supersonic shear layers induced by periodic Mach wave, *Physics of Fluids A*, Vol. 6, No. 3, 1645-1656, 1991.
- [17] L. M. Mack, On the inviscid acoustic-mode instability of supersonic shear flows, *Theoretical and Computational Fluid Dynamics*, Vol. 2, 97-123, 1990.
- [18] C. K. W. Tam, L. Auriault and F. Cambulli, Perfectly Matched Layer as an absorbing boundary condition for the linearized Euler equations in open and ducted domains, *Journal of Computational Physics*, 144, 213-234, 1998.

- [19] C. K. W. Tam and F. Q. Hu, On the three families of instability waves of high-speed jets, *Journal of Fluid Mechanics*, Vol. 201, 447-483, 1989.
- [20] C. K. W. Tam and J. C. Webb, Dispersion-relation-preserving finite difference schemes for computational acoustics, *Journal of Computational Physics*, Vol. 107, 262-281, 1993.
- [21] E. Turkel and A. Yefet, Absorbing PML boundary layers for wave-like equations, *Applied Numerical Mathematics*, Vol. 27, 533-557, 1998.
- [22] G. B. Witham, Linear and nonlinear waves, Willey, 1978.